The effect of solid particles on the heat transfer in a slurry pipe flow

Maria Teresa Scelzo[1,*], *Laura* Peveroni[1], *Delphine* Laboureur[1], and *Jean-Marie* Buchlin[1]

[1]von Karman Institute for fluid dynamics, Waterloosesteenweg 72, 1640 Sint-Genesius-Rode, Belgium

Abstract. This work discusses the results of the temperature measurements performed on a water-based slurry, seeded with polystyrene spherical particles and flowing in a heated horizontal pipe. The flow is fully turbulent, characterized by a Reynolds number between 4500 and 14000. Two particle size distributions are tested (with mean diameter of 0.35 mm and 0.85 mm respectively), which lead to homogeneous and heterogeneous flow regimes. A solid volume fraction up to 7% is reached. The results show that particles increase the liquid bulk temperature by lessening the mixture heat capacity. Moreover, the particles increase the liquid heat transfer coefficient. Additionally, in the bottom part of the pipe, the heat transfer coefficient behaves similarly to fluidised bed. Based on these results, a new semi-empirical correlation for the slurry Nusselt number in function of the relevant dimensionless groups of the problem (Reynolds and Prandtl numbers, density ratio, particles size to pipe diameter ratio and solid volume fraction) is proposed.

1 Introduction

Seeding the flow with solid particles has gained significant importance among the techniques to enhance the heat transfer capabilities of liquid and gas flows.

Small fraction of solids of particles at nano-scales in fluids produces an increase of thermal conductivity much higher than what is predicted by classical theory of slurry suspensions. The reason of this behavior is to be found not only in the increase thermal conductivity but also in the increased heat capacity, the increased effective heat transfer area, the intensified mixing and turbulence of the fluid. These phenomena are being exploited or proposed in many applications [1] such as heat exchangers [3] and nuclear reactors cooling [2].

Larger particles are encountered in fluidised bed applications. These systems are characterized by advantageous heating and cooling rates due to the enhanced mixing in the flow caused by the particles. The heat transfers in a fluidised bed are mainly radiative (particle-wall, particle-particle, and fluid-particle) and convective (particle- fluid), with a limited contribution of conduction (particle-particle or particle-wall) [4].

The effect of the solid volume fraction α on the convective heat transfer coefficient of a solid-liquid mixture flow (known as slurries) in pipes was first studied by Zisselmar et al. [5]. Experiments were performed with particles of mean diameter (d_p) between 12 μm and 120 μm, in a water slurry, at $Re_{D,l}$ between 88000 and 164000, where the subscript l indicates that the Reynolds number is calculated with the liquid phase properties. The data were analysed in terms of heat transfer coefficient enhancement (h^*), defined as:

$$h^* = \frac{h - h_l}{h_l} \tag{1}$$

where h is commonly defined as:

$$h = \frac{q''}{T_w - T_b} \tag{2}$$

with q'' being the provided heat flux, T_w the wall temperature and T_b the bulk temperature.

The experimental h^* showed a peak at $\alpha \approx 3\%$. The same conclusion was drawn by Ku et al. [6], who experimentally investigated the heat transfer coefficient of liquid-solid mixtures flowing in the inner pipe of a double pipe heat exchanger. Experiments were carried out using spherical fly ash particles with d_p between 0.4mm to 0.78 mm, α up to 50% and $Re_{D,l}$ between 4000 to 11000. The value of h increased with decreasing particle diameter and increasing volume concentration. However, for solid volume fractions higher than 15%, h^* reduced to negative values. In fact, if the solid volume fraction increases, the turbulence is hampered, and the heat transfer coefficient decreases.

Several correlations have been proposed for the slurry heat transfer coefficient in function of mixture properties and flow conditions. Table 1 shows the ones found in the literature and specifies the range of derivation and applicability. Similarly to the correlations in fully liquid conditions, the slurry heat transfer coefficient depends on Reynolds number (Re_D or $Re_{D,l}$) and the Prandtl number (Pr). Besides, the solid volume fraction must be taken into

*e-mail: scelzo@vki.ac.be

Table 1. Correlations for slurry heat transfer coefficient proposed in literature.

Ref.	α	D/d	Re	Pr	Correlation
	[-]	[-]	[-]	[-]	
[12]	0.002-0.012	282-10500	14000-140000	3.4-12.7	$\frac{h_l D}{k_l} = 0.131(\frac{DU\rho}{\mu})^{0.62}(\frac{C_{pl}\mu}{k_l})^{0.72}(\frac{k_p}{k_l})^{0.05}(\frac{D}{d})^{0.05}(\frac{C_{p_p}}{C_{p_l}})^{0.36}$
[10]	0.005-0.03	182-512	27000-120000	2.1-3.4	$\frac{hD}{k} = 0.202(\frac{UD\rho}{\mu_l})^{0.6}(\frac{Cp\mu}{k})^{0.675}(\frac{D}{d})^{0.092}(\frac{\mu}{\mu_l(T_w)})^{-1.95}$
[11]	0.01-0.1	14-147	8000-50000	-	$\frac{h_l D}{k_l} = 0.0161(\frac{DU\rho}{\mu})^{0.88}(\frac{C_{pl}\mu}{k_l})^{1/3}(\frac{\mu_l}{\mu(T_w)})^{-0.14}$
[6]	0.01-0.1	102-615	3000-11000	3.8-5	$\frac{hD}{k} = 0.0138(\frac{UD\rho}{\mu_l})^{0.772}(\frac{Cp\mu}{k})^{0.809}(\frac{D}{d})^{0.042}$

Table 2. Dimensionless numbers (num.) for heat transfer in slurries.

Re_D	$\frac{\rho U_{max} D}{\mu}$	Reynolds num.	$\frac{inertial forces}{viscous forces}$
Fr_d	$\frac{g d_p}{U_{max}}$	Froud num.	$\frac{gravity\ on\ particles}{flow\ inertia}$
α	$\frac{V_p}{V_p+V_l}$	Solid volume fraction	
β	$\frac{\rho_p}{\rho_l}$	Mixture density ratio	
	$\frac{v_{sl}}{U_{max}}$		$\frac{particles\ settling\ velocity}{flow\ velocity}$
	$\frac{d_p}{D}$		$\frac{particle\ diameter}{pipe\ diameter}$
Pr	$\frac{C_p k}{\mu}$	Prandtl num.	$\frac{momentum\ diffusivity}{thermal\ diffusivity}$
Nu_p	$\frac{h_{pl} d_p}{k_l}$	Nusselt num.	$\frac{convection\ fluid-particle}{conduction}$

account. Salamone et al. [12] and Harada et al. [11] included it in the slurry density ρ. Instead, Ku at al. [6] and Ozbelge et al. [8] made use of all the slurry properties such as the mixture viscosity (μ) and thermal conductivity (k) calculated as a function of the corresponding phases' properties and volume fraction. Finally, D/d_p is included in the correlations, but its power indicates that the dependency is rather weak, with respect to the other flow properties.

In this work, the analysis of the heat transfer coefficient enhancement bases on the temperature profile modification enabled by the particles. An analogy is proposed between the heat transfer enhancement of slurry pipe flows and fluidised beds, modifying the classical renewal cluster model. Finally, a new semi-empirical correlation is proposed that enables the prediction of the slurry heat transfer coefficient in a large range of flow conditions. The Section 2 reports the dimensionless numbers relevant to this problem. Section 3 describes the experimental facility, procedure, measurement techniques and the experimental uncertainty. The Section 4 shows the experimental results and the proposed semi-empirical correlations.

2 Slurry flow dimensional analysis

In order to identify the relevant quantities involved of heat transfer of slurry flows in pipes, the dimensionless form of the momentum and energy equations are derived. Under the assumption of steady, incompressible and 2D flow, the dimensionless momentum and energy equations read as in Eq.s 3-5. The reference dimensions are the pipe lenght (L, $\hat{z} = z/L$) and the pipe diameter (D, $\hat{y} = y/D$). The reference velocity in the axial direction is the maximum flow velocity U_{max} (i.e. $\hat{U}_{z,l} = U_{z,l}/U_{max}$) whereas the reference for the vertical component is the particles settling velocity v_{sl} (i.e. $\hat{U}_{y,l} = U_{y,l}/v_{sl}$). The reference pressure is the dynamic pressure $\rho_l U_{max}^2$ and the temperature is written in term of $\theta = \frac{T-T_m}{T_0-T_m}$.

The relevant dimensionless numbers derived from the previous equations are shown in Table 2 and are used in the analysis of the experimental results and in the derivation of the semi-empirical correlation for the Nu_D.

$$\hat{U}_{z,l}\frac{\partial \hat{U}_{z,l}}{\partial \hat{z}} + \frac{v_{sl}}{U_{max}}\frac{L}{D}\hat{U}_{y,l}\frac{\partial \hat{U}_{z,l}}{\partial \hat{y}} = \frac{\partial \hat{p}}{\partial \hat{z}} - \frac{1}{Re_D}\frac{D}{L}\frac{\partial^2 \hat{U}_{z,l}}{\partial \hat{z}^2} - \frac{1}{Re_D}\frac{L}{D}\frac{\partial^2 \hat{U}_{z,l}}{\partial \hat{y}^2} + C_D\alpha\frac{D}{d_p}\frac{L}{D}(\hat{U}_{z,l} - \hat{U}_{z,p})^2 \quad (3)$$

$$\hat{U}_{z,l}\frac{\partial \hat{U}_{y,l}}{\partial \hat{z}} + \hat{U}_{y,l}\frac{L}{D}\frac{v_{sl}}{U_{max}}\frac{\partial \hat{U}_{y,l}}{\partial \hat{y}} = \frac{\partial \hat{p}}{\partial \hat{y}}\frac{L}{D}\frac{U_{max}}{v_{sl}} - \frac{1}{Re_D}\frac{D}{L}\frac{\partial^2 \hat{U}_{y,l}}{\partial \hat{z}^2} - \frac{1}{Re_D}\frac{L}{D}\frac{\partial^2 \hat{U}_{y,l}}{\partial \hat{y}^2} + C_D\alpha\frac{D}{d}\frac{L}{D}\frac{v_{sl}}{U_{max}}(\Delta\hat{U}_{y,pl})^2 + (\beta-1)\frac{L}{D}\frac{D}{d_p}\frac{U_{max}}{v_{sl}}Fr^2 \quad (4)$$

$$\hat{U}_{z,l}\frac{\partial \hat{\theta}}{\partial \hat{z}} + \hat{U}_{y,l}\frac{L}{D}\frac{v_{sl}}{U_{max}}\frac{\partial \hat{\theta}}{\partial \hat{y}} = \frac{1}{PrRe_D}\frac{D}{L}\frac{\partial^2 \hat{\theta}}{\partial \hat{z}^2} + \frac{L}{D}\frac{1}{PrRe_D}\frac{\partial^2 \hat{\theta}}{\partial \hat{y}^2} + \frac{Nu_p}{PrRe_D}\frac{d_p}{D}\alpha(\hat{\theta_p} - \hat{\theta_l}) \quad (5)$$

3 Experimental methods

3.1 Facility and measurement techniques

The experiments discussed in this work were performed in the PREDICT facility of the von Karman Institute for fluid dynamics. The installation layout is shown in Figure 1(a).

The upstream feeding tank (1) is connected to the facility by means of an on-off valve (2). An electrical stirrer is activated to mix the slurry before and during the experiments, to facilitate the mixture to flow out, towards the test section.

The latter is a horizontal copper pipe (internal diameter D=30mm and wall thickness s=5mm), reported schematically in Figure 1(b). The horizontal segment is placed downstream the 45° bend and presents an entrance region of 17D to allow the flow establishment before entering the heated section. The heated test section extends for 2.5 m (corresponding to the red arrows in Figure 1). Electric resistive films (manufactured by Captec), glued around the copper pipe, provide constant wall heat flux through the Joule effect. The resistive foils are electrically supplied at 230 V with Solcon TPS31 power supply. The films, with a resistance of 5.3Ohm each, are placed on three balanced current phases connected in star configuration. This circuit provides heat power between 2.3 and 9.4 kW, corresponding to heat flux values ranging from 12 kW/m^2 to 60 kW/m^2. These high values of heat power enable temperature differences in the water flow higher than the measurement chain uncertainty for the whole range of mass flow rates.

The test section is instrumented with type K notsheathed thermocouples (Omega Engineering 5TC-TT-KI-36-1M). The sensing junction, immersed in the fluid, has a diameter of 0.13mm. The sensors are placed at six axial positions identified by the green arrows in Figure 1(b), three across the pipe test section (T_{up},T, T_{down}, in Figure 1(c)) and two for wall temperature measurement ($T_{w,up}$, $T_{w,down}$ in Figure 1(c)). The resistive films feature holes to allow inserting the thermocouples along the heated section. The sensors are glued on a rigid metallic bar, screwed in the pipe, at the measurement positions. In particular, the wall temperature measurements are achieved with two opposite sensors placed in such a way that the sensing junction results flush mounted with respect to the inner pipe surface. The results presented in this work hing on the measurements performed in the last axial position.

Along the test section three glass windows (GPE Scientific Ltd), identified with the blue arrows in Figure 1, allow qualitative visualisation of the flow regime and quantitative assessment of the solid volume fraction. The glass windows have a length of 110mm and internal diameter of 30mm. The first glass insert is placed at the onset of the heated section to monitor the inlet conditions; the second and the third glass inserts are placed a distance of 1000 mm from each other, the last being at the outlet section. The images are recorded with a Phantom v.7 high speed camera, with a 60mm macro Nikon objective.

On the vertical segment, the Coriolis meter (Yokogawa) transmits the values of mass flow rate and flow density to the digital acquisition system.

Downstream the flow regulation valve (Figure 1 (5)), a filter collects the solid particles separated from the slurry, while a returning circuit with a pump (7) recirculates the water for the whole duration of the test.

Table 3 reports the properties of the two phases of the working slurry, water and polystyrene spherical particles.

3.2 Experimental procedure

Figure 2 shows an example of mass flow rate, inlet and outlet temperatures evolution during one experiment. Before starting the test, the facility is filled with water at ambient temperature. When the on-off valve is opened, water only starts flowing in the facility and once the mass flow rate reaches a constant value, the heaters are switched on ($t \approx 20s$ in Figure 2).

The amount of power is modulated depending on the mass flow rate to avoid reaching the maximum temperature allowed by the heating films (120 $°C$). Particles are injected in the feeding tank and enter the test section only after the thermal steady state in fully liquid flow is reached ($t \approx 165s$ in Figure 2). It is worth noting that the buffer tank is big enough to ensure constant inlet temperature during the experiments (black line in Figure 2).

3.3 Uncertainty quantification

The heat transfer coefficient h derives from the temperature measurements according to Eq.2, where $q^{"}$ is the imposed heat flux calculated as in Eq. 6,

$$q^{"} = \dot{m} c_p (T_{b,out} - T_{b,in}) \tag{6}$$

with $\dot{m}$ being the mass flow rate and c_p the mixture specific heat capacity. The bulk temperature is calculated from the six radial temperature measurements as in Eq. 7

$$T_b(x) = \frac{1}{D} \int_0^D T(y) dy \tag{7}$$

Therefore, the uncertainty on h reads as:

$$\frac{\delta h}{h} = \sqrt{\left(\frac{\delta(T_w - T_b)}{T_w - T_b}\right)^2 + \left(\frac{\delta(T_{out} - T_{in})}{T_{out} - T_{in}}\right)^2} \tag{8}$$

Bias uncertainty on the mass flow rate ($0.5\% rdg$) is negligible with respect to the temperature measurement contributions. Moreover, the uncertainty of each measured quantity accounts the statistical error that derives from averaging the quantity on about 20 seconds of steady state.

Figure 3 shows the expected uncertainty on the value of h depending on the temperature difference achieved between the pipe wall and the bulk flow $\Delta T = T_w - T_b$. As expected, diminishing ΔT produces higher uncertainty on the heat transfer coefficient values. To achieve the desired high values of ΔT, a specific heat power must be provided

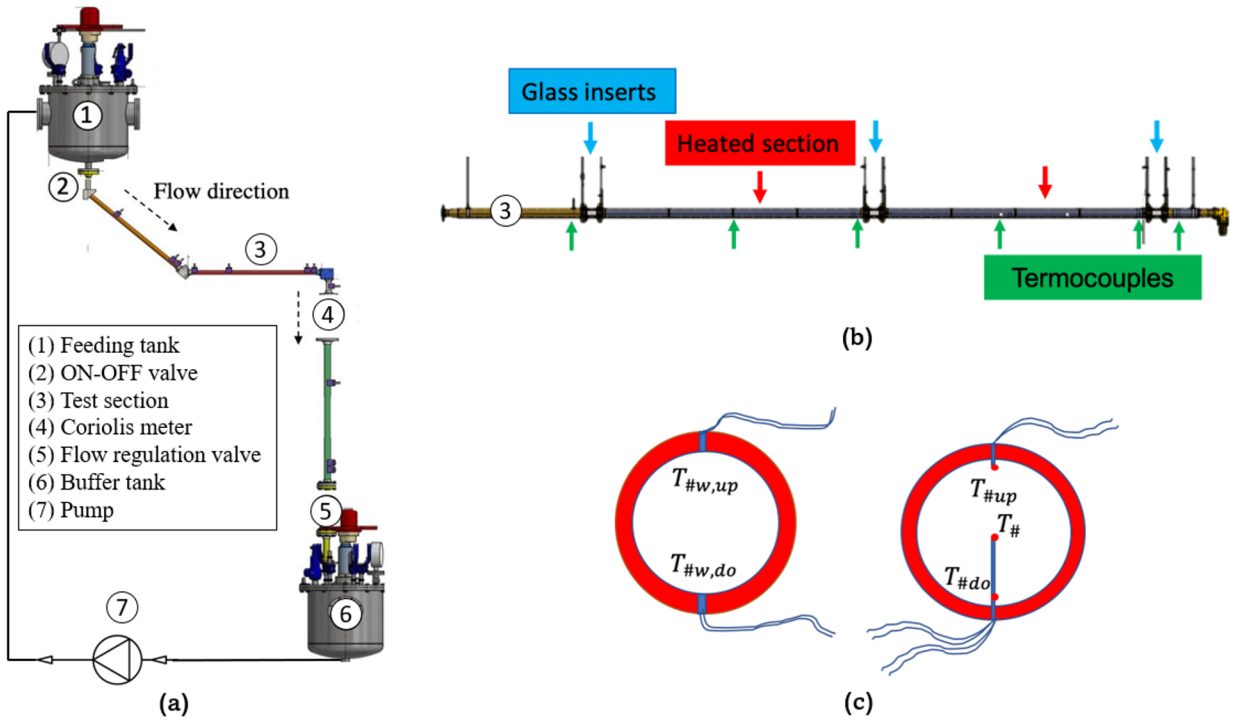

Fig. 1. (a) Schematic of the PREDICT installation, (b) test section, (c) radial position of the thermocouples at each of the six axial measurement positions.

Table 3. Properties of the slurry components: water and polystyrene particles.

	ρ $[kg\,m^{-3}]$	μ $[Pa\,s]$	d_p $[mm]$	k $[W\,m^{-1}K^{-1}]$	c_p $[J\,kg^{-1}K^{-1}]$
Water	999	0.001	-	0.6	4186
Particles	1050	-	0.35-0.85	1.33	1339

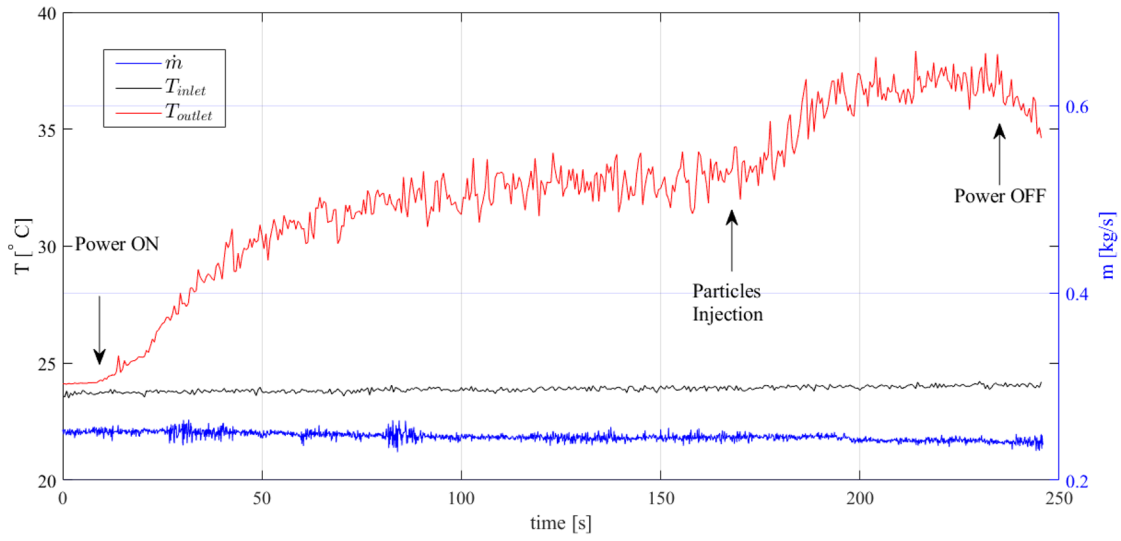

Fig. 2. Mass flow rate and inlet and outlet temperature evolution during a test for heat transfer coefficient measurement.

to the test section, depending on the flow Reynolds number, as illustrated in Figure 4. The power supply provides current intensity high enough to enable the lowest value of uncertainty on the heat transfer coefficient value (corre-

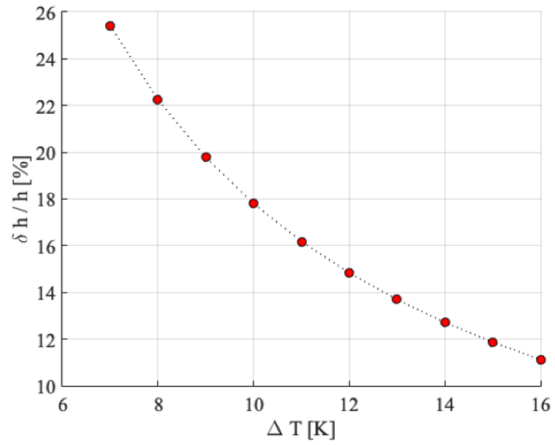

Fig. 3. Uncertainty on the heat transfer coefficient values in function of the temperature difference between pipe wall and bulk temperature

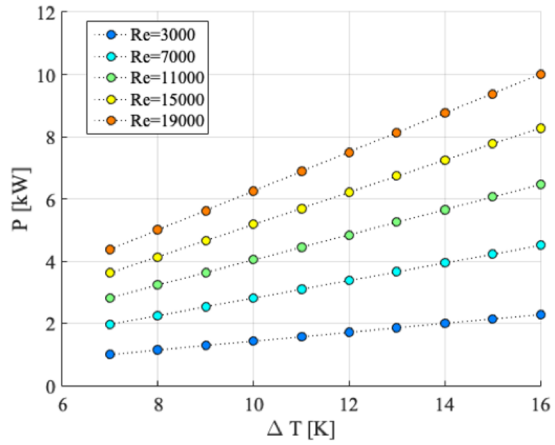

Fig. 4: Heat power (P) required to achieve a desired ΔT between wall and bulk fluid for different values of Reynolds number (Re).

sponding to $\Delta T = 16°C$) for all the flow conditions. On the other hand, the heat power during the experiments is constrained by the maximum temperature achievable on the heating films' surface, $120°C$, thus, it is modulated depending on the flow Reynolds number. This test approach results in a ΔT around $9°C$, leading to an expected uncertainty on h of around 20% for the entire range of Reynolds number.

4 Results

4.1 Flow regimes identification

Figure 5 shows four exemplary video frames acquired in background lighting configuration, for $\alpha \approx 1\%$ and $\alpha \approx 5\%$, and d_p=0.35mm and d_p=0.85mm. It is worth noticing that for the same Reynolds conditions, different particle distribution establish depending on the particle size. In fact, the flow regime depends on the ratio between the particles traveling time ($t_p = D/2v_{sl}$) and flow time scale ($t_f = L/U$). Since the test section dimension (D) does not change nor the location of the visualization window (L), the flow dynamics is regulated by the ratio between the settling velocity (proportional to d_p) and the slurry flow velocity, as anticipated in Section 2.

The homogeneous suspension occupies the whole test section and exhibits a symmetric particles velocity profile with respect to the pipe cross section. On the other hand, particles moving as heterogeneous suspension or moving bed are located in the lower half of the pipe. The moving bed features a substantial reduction of the velocity in proximity of the wall.

4.2 Temperature profiles modification

Figures 5 show the comparison between liquid temperature profile in fully liquid conditions and in presence of particles (referred to as slurry temperature profile) corresponding to four different flow conditions. The two profiles derive from the same experiments, *i.e.* they feature the same heat power and mass flow rate. In all the cases, the slurry temperature (blue line in Figures 5 (b-d-f-h)) is higher than the fully liquid conditions (red line in Figures 5(b-d-f-h)).

For fully suspended slurry (Figure 5 (e-f)-(g-h)), the presence of particles leads to an uniform increase of the temperature along the pipe cross-section. On the other hand, when the distribution of particles is heterogeneous (Figure 5 (c-d)), the slurry temperature shows an increase at the bottom half of the pipe higher than at the upper positions. Hence, it can be concluded that the temperature enhancement depends on the slurry solid content.

According to the energy balance, at a fixed heat flux and slurry mass flow rate, the slurry exhibits higher outlet temperature than the liquid flow because of the decreased specific heat capacity. The temperature enhancement is expressed by Eq. 9.

$$[T - T_l]_{out} = \frac{q'' \pi D L}{\dot{m}} \left(\frac{1}{c_p} - \frac{1}{c_{pl}} \right) \tag{9}$$

being T and T_l the bulk temperature at the outlet section, evaluated as in Eq. 7, respectively in slurry liquid conditions.

Figure 6 shows the comparison between the expected enhancement of the temperature profile $[T - T_l]_{out}$ and the one calculated from the experimental temperature profiles. The vertical error bars represent the experimental uncertainty of the quantity $[T - T_l]_{out}$.

In order to combine the effect of the mass flow rate and the solid volume fraction, the experimental data are classified according to a modified Froude particle number (Fr^*) expressed in Eq. 10.

$$Fr^* = \frac{U^2}{g d_p} \frac{\rho_l}{\rho} = \frac{U^2}{g d_p} \frac{1}{1 + (\beta - 1)\alpha} \tag{10}$$

This quantity is the particle Froude number, defined in Section 2, multiplied by the ratio between the liquid and

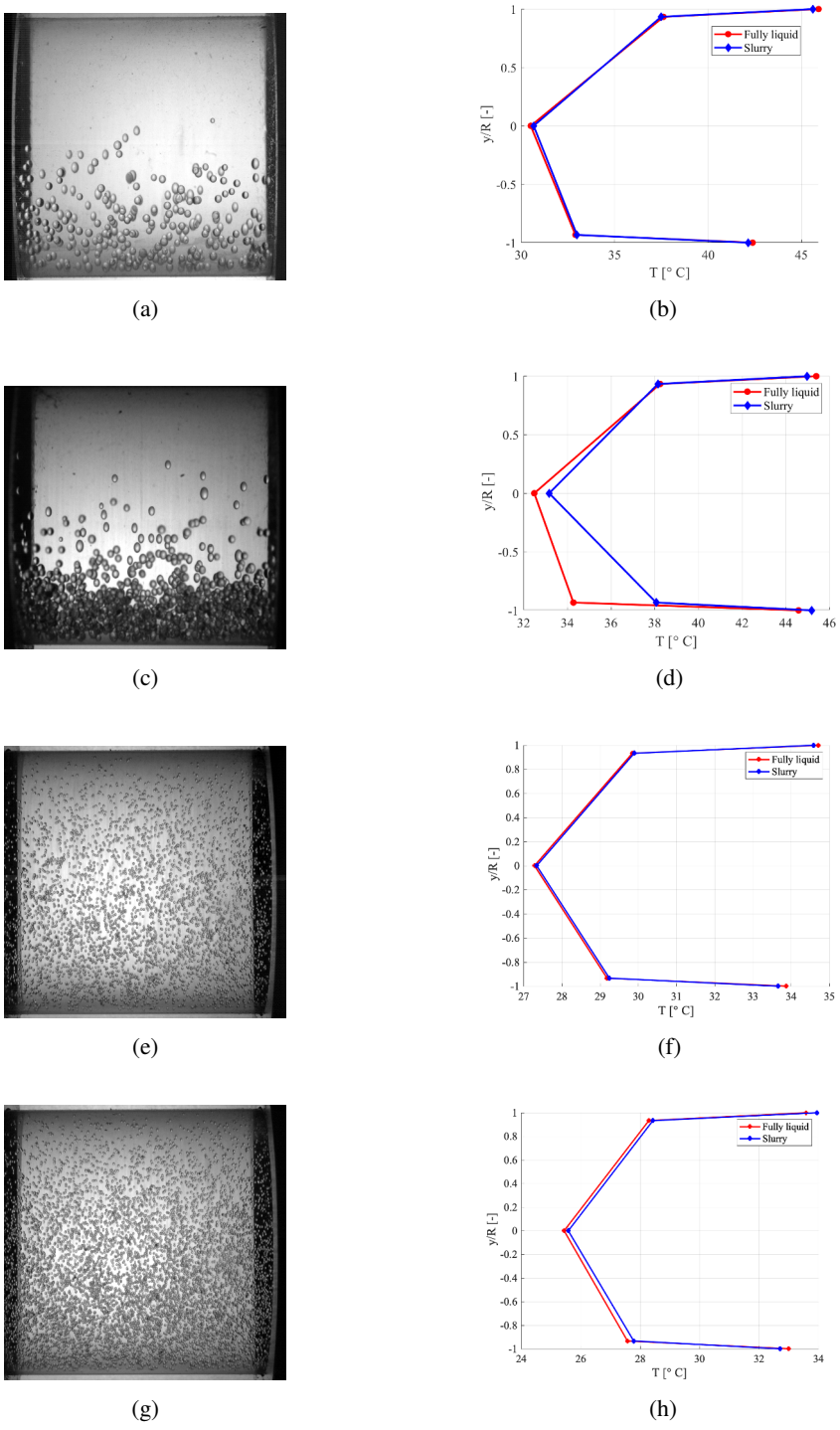

Fig. 5. Video frames of slurry and temperature profiles at $Re_D \approx 10000$ (a-b) $\alpha \approx 1\%$, d_p=0.85mm, N_e=130, heterogeneous suspension;(c-d) $\alpha \approx 5\%$, d_p=0.85mm, N_e=60, moving bed; (e-f) $\alpha \approx 1\%$, d_p=0.35mm, N_e=410, homogeneous suspension; (g-h) $\alpha \approx 5\%$, d_p=0.35mm; N_e=200, homogeneous suspension.

the slurry density (ρ_l/ρ) that can be expressed in terms of solid volume fraction α and the density ratio β. Hence, Fr^* represents the ratio between the liquid flow inertia and the gravitational effect on the particles. According to the definition, Fr^* decreases at low mass flow rate and high solid volume fraction which favor the settling of the solid particles. At Fr^* higher than 10 (red marks in Figure 6), the experimental points fairly align on the behavior predicted by Eq. 9 (black line in Figure 6). On the other hand, for most of the points at lower values of Fr^* (black marks in Figure 6), the particles undergo strong settling toward the bottom pipe wall where the flow velocity decreases and the solid volume fraction increases. These conditions corresponds to the moving bed regime and cause an overheating of the

lower part of the pipe. Hence, the bulk temperature deviates from the expected behaviour predicted by Eq.9. It is important to notice that the most relevant parameters in the definition of Fr^* are the flow velocity and the particle size, being the density ratio and the solid volume fraction relatively low. Therefore, there are cases of experiments at $Fr^* < 10$ that correspond to a dispersed distribution of particles and do not exhibit moving bed regime.

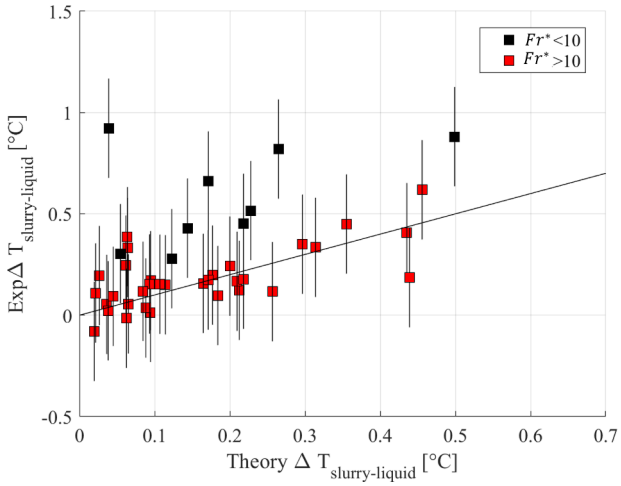

Fig. 6. Comparison between theoretical and experimen-tal $\Delta T_{slurry-liquid}=[T - T_l]_{out}$ in function of the modified Froude number Fr^*.

4.3 Heat transfer coefficient prediction

As reported in the introduction, the high heat transfer coefficient is one of the greatest advantages of fluidised bed [4]. An analogy can be established between the fluidised bed and the present experimental results with d_p=0.85mm, for which the particles settle at the pipe bottom wall. To this end, Figures 7 show the ratio between slurry and fully liquid heat transfer coefficient calculated for the upper (a) and lower (b) half of the pipe, in function of the average solid volume fraction. The heat transfer coefficients (h_{slurry} and h_{liquid}) are defined as:

$$h_{up,down} = \frac{q''}{T_{wallup,down} - \frac{1}{R}\int_0^{R/2} T dy} \tag{11}$$

In the upper part of the pipe the wall is always particles free, hence, the ratio h_{slurry}/h_{liquid} does not depend on α nor on $Re_{D,l}$ and it is close to 1. For the bottom part of the wall, higher values α enable greater h_{slurry}/h_{liquid}. In Figure 7 the data are classified according to the Re_D: it is found that lower flow velocities correspond to higher relative heat transfer coefficient. High values of α and low values of Re_D can be considered altogether looking at the solid volume fraction at the bottom part of the pipe α_{down}. In fact, for low $Re_{D,l}$ values, the particles accumulate close to the wall increasing α_{down}. At higher $Re_{D,l}$, instead, the particles distribute uniformly across the section. Thus, it is interesting to note the consistent increase of h_{slurry}/h_{liquid} in function of α_{down} shown with the blue marks in Figure 8(a).

According to Basu and Nag [4], the heat transfer coefficient in a fluidised bed can be predicted by a renewal cluster model. In a circulating fluidised bed clusters of particles alternate at the furnace bottom part due to the upward gas flow through the wall. Therefore, the total heat transfer at the wall is constituted by an unsteady heat conduction component h_p and a fluid convection component h_l. The two factors are weighted on the wall coverage fraction defined by the empirical correlation $f = 3.5\alpha^{0.37}$. In formulae the total heat transfer coefficient reads:

$$h_{tot} = f h_p + (1 - f) h_l. \tag{12}$$

with:

$$h_p = \frac{1}{\frac{d_p}{\delta k_l} + \sqrt{\frac{t\pi}{4kC_p\rho_p}}}; h_l = \frac{k_l}{d_p}\frac{C_p}{C_{p,l}}\left(\frac{\rho_l}{\rho_p}\right)^{0.3}\left(\frac{v_{sl}^2}{g d_p}\right)^{0.21} \tag{13}$$

where t is the residence time of the clusters at the wall, δ is the liquid layer thickness between the particles and the wall k_l is the thermal conductivity of the continuous phase and k, c and ρ_p are the properties of the mixture calculated according to α_{wall}. For the present application, the residence time t is evaluated as the contact time of the particles with the wall and it is defined as $t = 1/U$ and δ is negligible with respect to the particles diameter. Moreover, the radiation component to the heat transfer is not taken into account because the temperatures are very low compared to the fluidised bed operating conditions.

Finally, an additional convective term should be considered for the analysis of slurry flows. This can be defined as $h_s = Nu_{s,D}D/k_s$ where $Nu_{s,D}$ is calculated with the Dittus-Boetler correlation using the mixture properties, function of α_{down}. Therefore, the total heat transfer coefficient between the wall and the particulate reads:

$$h_{tot} = f h_p + (1 - f) h_l + h_s \tag{14}$$

To bound the values of the clusters wall coverage between 0 and 1, a modified formulation of f is proposed and reads:

$$f = \begin{cases} 3.5\alpha_{down}^{0.37} & if \alpha_{down} < 0.1 \\ 1 & if \alpha_{down} > 0.1 \end{cases} \tag{15}$$

The value of h_{tot} predicted by Eq. 14 is reported in Figure 8(a), shown with red marks, in terms of h_{slurry}/h_{liquid} in function of α_{down}. This semi-empirical model provides a fairly good prediction of the heat transfer in the bottom part of the pipe with a maximum deviation of 20% (Figure 8(b)). It is worth noticing that the unsteady conductive term h_p plays a minor role in slurry flows because the residence time is relatively high ($0.2sec$). Finally, the dependency of h_{slurry}/h_{liquid} on the flow velocity, for example at $\alpha_{down} < 5\%$, is provided by the additional convective term h_s that is peculiar to slurry flows and not present in fluidised bed.

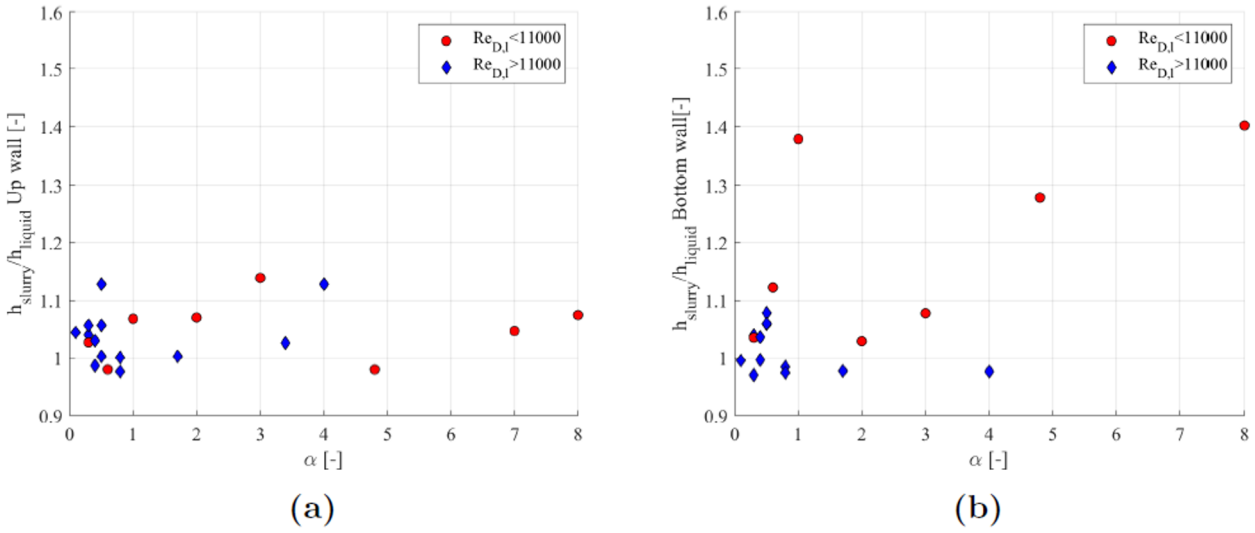

Fig. 7. Slurry heat transfer coefficient enhancement with respect to the single phase fully liquid flow (a) in the upper half of the pipe and (b) in the lower half of the pipe, in function of the solid volume fraction.

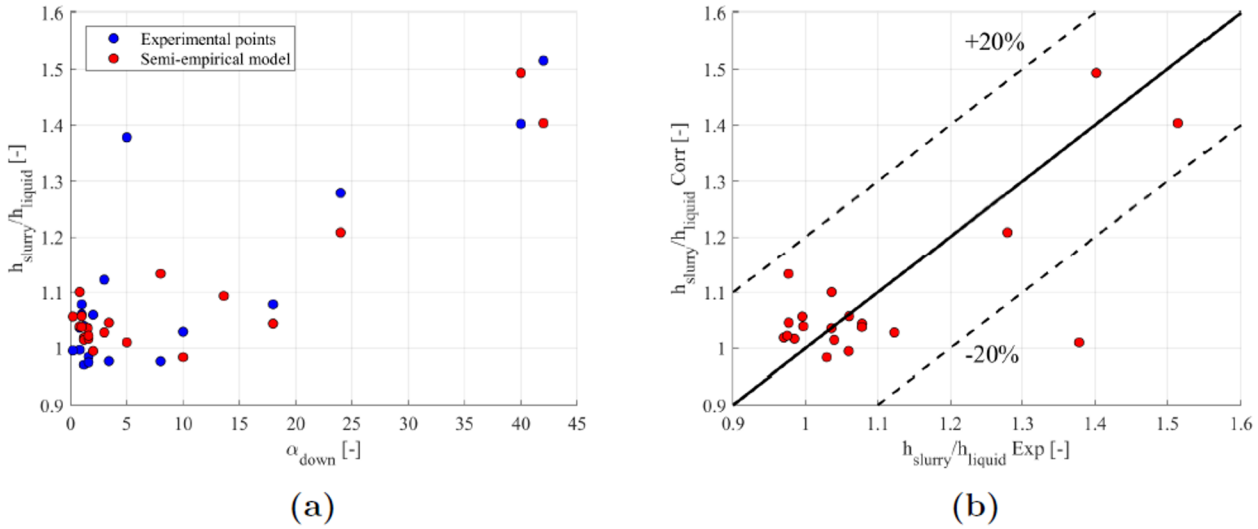

Fig. 8. Slurry heat transfer coefficient enhancement in function of α_{down} (blue marks) and prediction obtained with a modified semi-empirical model for fluidised bed (red marks). (b) Deviation between the experiments and the semi-empirical model.

Concerning the global heat transfer coefficient, attempts to predict the experimental slurry Nusselt number have been made with previous correlations. The correlation proposed by Ku et al. [6] and the one proposed by Ozbelge et al. [10], do not fit the present experimental conditions, therefore, they may be not applicable. The only suited correlation is proposed by Harada et al. [11], even though it does not take into account the particles size, and it ultimately underestimates the values of Nu_D found in the experiments.

Therefore, it appears worthwhile seeking for a new semi-empirical correlation function of the relevant parameters of the problem, the liquid $Re_{D,l}$, the liquid Pr_l, the particle to pipe diameter ratio (d_p/D), the solid volume volume fraction (α) and the density ratio (β), as indicated by the dimensionless equations reported in Section 2. The correlation is built with a Minimum Searching Optimization Algorithm, imposing constraints on the power of $Re_{D,l}$ and Pr_l. The correlation is formulated as follow:

$$\frac{hD}{k_l} = 0.077 Re_{D,l}^{0.71} Pr_l^{0.68} \left(\frac{d_p}{D}\right)^{0.12} \alpha^{-0.07} \beta^{-1.2} \qquad (16)$$

Figures 9 show the prediction of the present experimental Nusselt number in the upper half of the pipe and in the bottom half of the pipe, respectively with h_{down} and h_{up} calculated as in Eq. 11.

Moreover, Figure 10 shows the comparison between literature data from Ozbelge [8] and Ku [6] and the values

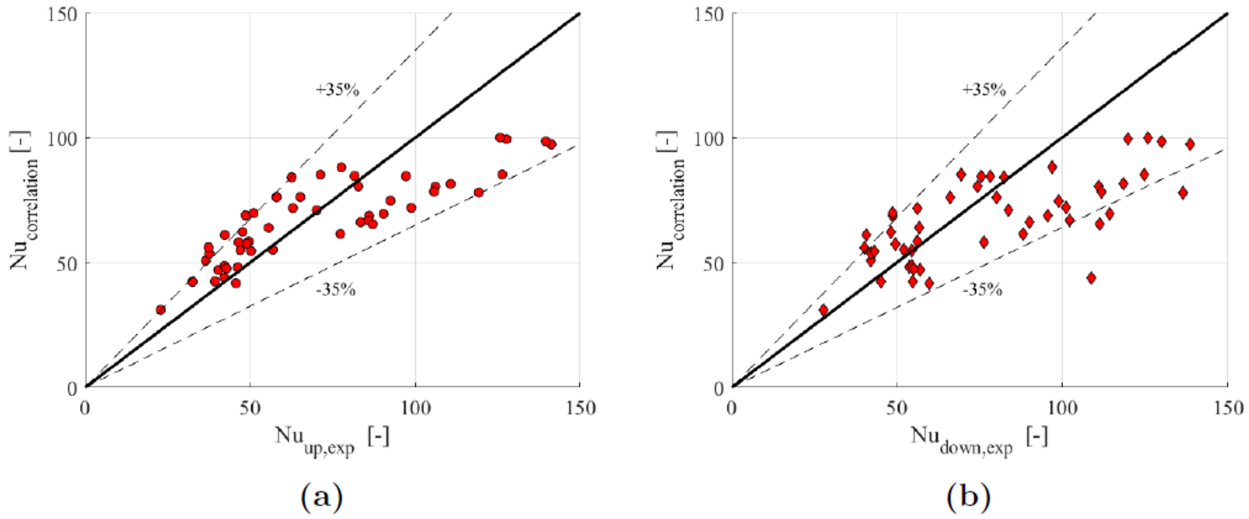

Fig. 9. Comparison between Eq. 16 and experimental values of Nusselt number Nu_D calculated (a) in the upper half of the pipe and (b) in the bottom half of the pipe.

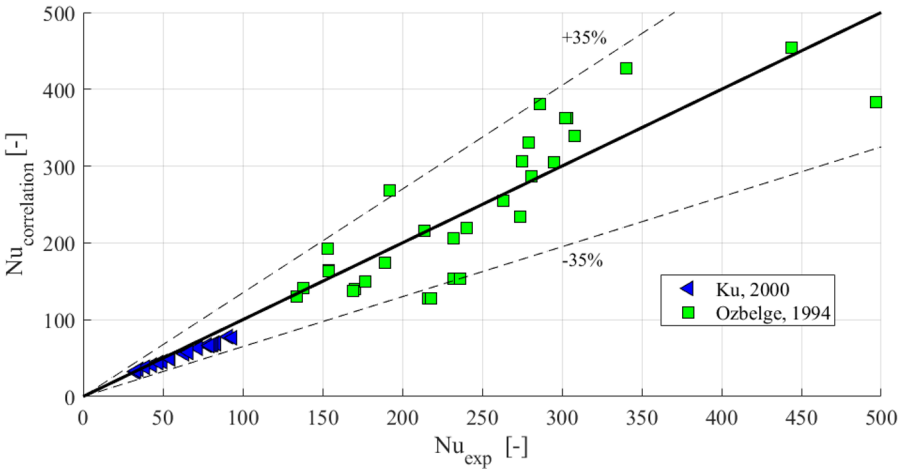

Fig. 10. Comparison between Eq. 16 and the data from Ozbelge [8] and Ku [6].

predicted by Eq. 16. The proposed correlation yields satisfactory prediction within the 35 % of deviation from the literature data. Contrarily to the previous correlations, the effect of the solid volume fraction is not included in the definition of Re_D and Pr leading to lower uncertainties on the evaluation of fluid properties and ultimately on the predicted Nu_D. Moreover, the present formulation explicitly includes the density ratio β.

5 Conclusions

The study of the slurry flow in non-isothermal conditions aimed to analyze the effect of the solid particles on the flow heat transfer coefficient. The working fluid is a water-base slurry seeded with polystyrene particles of d_p = 0.85mm and d_p = 0.35mm, enabling moving bed, heterogeneous and homogeneous flow regimes. The effects of the solid particles on the heat transfer features of the liquid carrier are the following.

- The particles increase the flow bulk temperature with respect to the fully liquid conditions because they diminish the fluid specific heat. A modified Froude number is defined to classify the temperature enhancement behavior: at $Fr^* > 10$ the particles are fully suspended and the bulk temperature increases proportionally to α according to the energy balance. At $Fr^* < 10$ the experimental points deviate from this behavior because the massive presence of particles in the lower part of the pipe causes an asymmetrical overheating of the flow.
- The experiments showed that the slurry heat transfer coefficient is always higher than the fully liquid flow, at the same mass flow rate and wall heat flux.
- In the bottom part of the pipe, where particles accumulate because of the gravity force, the heat transfer coef-

ficient behaves similarly to fluidised bed. The renewal cluster model [4] is modified to account for the advective contribution of the slurry flow, achieving the prediction of the experimental data within the 20% deviation.

- A new semi-empirical correlation (Eq. 16) is proposed for the prediction of the slurry heat transfer coefficient in function of the relevant dimensionless groups of the problem, Re_{Dl}, Pr_l, d_p/D, α, β. The correlation predicts, within 35 % of dispersion, the data reported by Ku et al [6] and Ozbelge et al. [8], hence, it is applicable for Re_{Dl} between 3000 and 140000, Pr between 2.1 and 7, α up to 10% and D/d_p between 14 and 1050.

Acknowledgement

This work was supported by ESA-ESTEC (European Space Agency - European Space Research and Technology Centre) through the Networking/Partnering Initiative. This work was performed in the framework of M.T. Scelzo's PhD thesis funded by the Fonds de la Recherche Scien-tifique F.R.S.-FNRS through the FRIA grant, and by the von Karman Institute for fluid dynamics.

References

[1] Saidur, R., Leong, K. Y., Mohammed, H. A. Renewable and sustainable energy reviews, 15(3), 1646-1668, (2011).

[2] Buongiorno, J., Hu, L. W., Kim, S. J., Hannink, R., Truong, B. A. O., Forrest, E. Nuclear Technology, 162(1), 80-91 (1979).

[3] Huminic, G., Huminic, A. Renewable and Sustainable Energy Reviews, 16(8), 5625-5638 (2012)

[4] Basu, P. and Nag, P.K., M., Chemical Engineering Science, 51, 1 (1996)

[5] Zisselmar, R., Molerus, O., Elsevier, J. Chem. Eng., 18, 7 (1979)

[6] Ku, J.-H. and Cho, H.-H. and Koo, J.-H. and Yoon, S.-G.and Lee, J.-K., Springer, KSME INT J,14,10 (2000).

[7] Brandon, C. A. and Thomas, D. G., Proc. 4th Int. Heat Transfer Conf. Paris (1970)

[8] Ozbelge, T.A., Int. J. Multiphase Flow, 19, 3 (1993)

[9] Ozbelge, T.A and Somer,G., J. Chem. Eng.,38 (1988)

[10] Ozbelge, T.A and Somer,G., J. Chem. Eng.,55 (1994)

[11] Harada, E. and Toda, M. and Kuriyama, M. and Konno, H., J. Chem. Eng. Jpn., 18, 1 (1985)

[12] Salamone, J. J. and Newman, M., Industrial & Engineering Chemistry, 47, 2 (1955)